Charge exchange at molecular-orbital pseudocrossings as an important mechanism for nonkinetic-electron emission in slow-multicharged-ion ($v < v_0$) metal-surface scattering

K. J. Snowdon,* C. C. Havener, F. W. Meyer, S. H. Overbury, and D. M. Zehner
Oak Ridge National Laboratory, Oak Ridge, Tennessee 37831

W. Heiland
Fachbereich Physik, Universität Osnabrück, 4500 Osnabrück, West Germany
(Received 21 September 1987; revised manuscript received 16 February 1988)

Kinetic energy distributions of electrons emitted in the interaction of slow ($10q$-keV) multicharged ions (N,O,Ne,Ar) with metal surfaces (Cu,Au) are presented. We observe secondary-electron emission, quasielastic-scattering processes, and, superimposed upon this, one-center Auger decay of both projectile and target vacancies. Two classes of target Auger-decay features are observed. Long-lived target vacancies decay, leading to discrete Auger line features, similar to those arising from electron-impact excitation. Short-lived target vacancies appear to decay in the field of the projectile, leading to broadened Auger line features. Observation of the decay of target vacancies, and their correlation with the presence of particular projectile vacancies, shows that a measurable fraction of projectile vacancies survive until small-impact-parameter collisions with surface or subsurface atoms. The data imply that projectile neutralization proceeds via two channels, viz., capture of valence-band electrons to projectile excited states, followed by one-center Auger decay, and at pseudocrossings of molecular orbitals correlating with discrete inner-shell levels of the target and projectile.

I. INTRODUCTION

Several early observations of electron yields from slow ($v < v_0$) multicharged-ion–metal-surface scattering, as a function of projectile charge state, established a linear relationship between electron yield and total neutralization energy in the ion.[1,2] Only the presence of deep-lying core vacancies on the projectile create deviations from this general rule.[3,4] These observations are consistent with a theoretical model proposed by Arifov *et al.*,[5] in which the primary mechanism of charge exchange is transfer of target valence electrons to high-lying projectile excited states, which subsequently relax via one-center Auger decay, leading to the observed electron emission. This model has received support from measurements of the electron energy distribution arising from the collision of doubly charged ions with metal surfaces.[2,6]

Attractive as this model is, it remains an open question whether, for a highly charged ion, sufficient time exists on the approach trajectory for decay of all projectile vacancies. While some Auger transitions occur on time scales of order $10^{-16}s$, others are, for example, forbidden by selection rules. The survival of inner-shell vacancies up to small-impact-parameter collisions would open the possibility of molecular-orbital pseudocrossings involving target inner-shell levels, with consequent vacancy transfer. That such transfer occurs for K-shell vacancies has recently been verified by Meyer *et al.*[7] The additional possibility that projectile inner-shell vacancies even survive the close collision with target atoms has been provided by de Zwart *et al.*[3] via measurements of the dependence of projectile final charge state on projectile initial charge.

Outer-shell discrete states of the projectile also couple efficiently to discrete states of metal targets. Indeed, this was one of the very earliest observations in the field of low-energy ion-surface scattering.[8] In view of this fact, it is perhaps timely to ask whether the currently accepted mechanism for the neutralization of multicharged ions, namely, the process whereby target *valence* electrons transfer to projectile discrete states, represents the primary or only charge transfer channel for such states.

We wish in this paper to distinguish experimentally the various possible mechanisms of charge transfer to multicharged projectiles in collision with metal surfaces. Electrons emitted from the projectile, moving *above* the target surface, either before or after the collision, will be Doppler shifted in the laboratory frame. In the absence of anisotropies in the electron pickup, electrons emitted from the projectile following one-center Auger decay will exhibit an angular distribution essentially isotropic in the projectile frame. Projectile electrons emitted on the incident trajectory are emitted during the interaction and will have energies perturbed by that interaction. Postcollision relaxation (well beyond the surface) will exhibit discrete line emission.

On the other hand, electrons emitted from the decay of target atoms in the solid matrix, or from implanted projectile ions, will be characteristic of the solid state (i.e., exhibit chemical shifts), will be broadened if emitted during the collision, and will have, external to the surface, a close to cosine angular distribution. To distinguish these charge transfer channels and collision regions (incident trajectory, hard collision, postcollision) we require experiments using the following.

(i) A variety of projectiles. The model of Arifov predicts the electron emission will be characteristic of Auger transitions involving projectile states.

(ii) Several target materials. The molecular-orbital pseudocrossing model predicts the electron emission will reflect Auger transitions in the target.

(iii) Variable observation geometry. The near isotropic (at low projectile velocity) and cosine angular distributions of the projectile and target emissions, respectively, make their separation possible. Observations near parallel to the surface discriminate against target and implanted projectile emission. Observations at other angles contain contributions from both target and projectile.

(iv) High energy and angular resolution. The high energy resolution is necessary to distinguish discrete from broadband emission, the high angular resolution to reduce Doppler broadening of projectile-Auger peaks.

In Sec. II we describe an apparatus fulfilling the above requirements.

II. EXPERIMENTAL APPARATUS

The experiments utilize beams from the Oak Ridge National Laboratory (ORNL) electron cyclotron resonance (ECR) multicharged-ion source.[9] This source produces high charge state ion beams ranging from fully stripped light ions ($Z<10$) up to 40% stripped heavy ions ($Z\approx 80$), including the metallic ions Cr, Fe, Ni, Ta, and Au. Representative beam currents for a source extraction voltage typically used in these experiments are shown in Table I. After charge selection and focusing, the beam enters an ultrahigh-vacuum chamber (base pressure 10^{-10} torr) through a 0.76-mm-diam aperture. The measured beamwidth at the target position was 0.7 ± 0.1 mm full width at half maximum (FWHM).

The beam was incident on the (110) surfaces of gold and copper single crystals mounted at different times on a two axis goniometer. The crystals, of 99.999% purity, were spark cut, polished with alumina paste, and oriented to within 0.2° using back Laue x-ray techniques. The samples were then electrochemically polished and the copper sample was annealed in a hydrogen atmosphere at 700 °C and 1 atm for several days to remove residual bulk sulfur impurities. Before each experiment, the surfaces were sputter cleaned using 1 keV Ne^+ at 10° incidence to the surface, annealed, and their cleanliness monitored using electron-induced Auger electron spectroscopy.

The crystal target mount was isolated from ground. The electrical current to the target, equal to the sum of incident ion beam current and ejected electron current, could therefore be monitored and used for normalization purposes. In the present experiment the relative contributions of ejected electrons and incident ions to the target current were not determined. Previous measurement[7] at similar energies and grazing angles of incidence had shown that, for a Au target, the ejected electron yield per incident ion was $\gg 1$, and that the measured target current for that case was therefore predominantly due to emitted electrons.

The energy distributions of emitted electrons arising from the multicharged ion-surface interaction were measured using a cylindrical mirror analyzer (CMA), equipped with an electron gun, and operating in particle counting mode. The CMA pass energy and data collection were controlled by a minicomputer-based multichannel scaler. The dwell time per channel was normalized by integrating the target current to a preset charge. The CMA electron multiplier was operated with a front-end bias of + 500 V with respect to the CMA final aperture to enhance the detection efficiency for low-energy electrons. The magnetic field in the interaction region was reduced to less than 10^{-1} G by the use of Helmholtz coils. The electron-induced secondary-electron energy distribution measured from Au using this arrangement exhibits a peak at 1.8 eV (Fig. 1), close to that expected theoretically ($\Phi/2$, where Φ is the metal work function[10,11]).

Most measurements were performed using the geometrical arrangement shown schematically in Fig. 2. The ion beam was incident at 5° to the surface plane. For the stated beam diameter, this results in an extended electron source of dimension 0.7×8 mm^2. It is well known that an extended electron source degrades the energy resolution of a CMA.[12,13] To determine the extent of this effect, we compared in Fig. 3 the widths of the electron-induced (small source) and ion-induced (extended source) Au *NVV* feature. This feature has a natural width of order twice the valence-band width or 11.2 eV for Au. The electron-induced spectrum has essentially this width consistent with the nominal $0.012E$ resolution of the CMA (where E is the electron energy). Using the measured widths of the ion-induced Au *NVV* and Au *NNV* peaks (Fig. 3), and the known natural widths of these peaks, we determine an upper limit for the instrumental resolution, *for this geometry and a stationary emitter,* to be $0.16E$. A slight difference between the energy calibration for electron-induced and ion-induced target emission was observed (Fig. 3). The origin may be that the transmission characteristics of an extended source at 85° to the CMA axis favor lower energies than the nominal pass energy. Despite this, we use throughout this work the absolute energy scale calibration established using elastic scattering of a known energy focused electron beam.

The CMA transmits electrons emitted in the polar angular range $36°<\theta<48°$, measured with respect to the CMA axis. Thus measurements at the laboratory energy E contain a range of electron energies measured with respect to the center of mass of a moving emitter (Doppler effect). The calculated Doppler profile of oxygen *KLL* electrons neglecting instrumental broadening, for the geometry of Fig. 2 and a projectile energy of 70 keV, is shown in Fig. 4. Both the Doppler and instrumental widths can be radically reduced (at the expense of sensitivity) by the introduction of a slit at the entrance to the CMA. A slit of 1.6 mm (with long axis oriented perpendicular to the plane defined by the ion beam and the surface normal) was used for detailed higher-resolution studies of projectile Auger electron spectra.

To enable a clear separation of projectile and target electron emission, we utilize such a slit in front of the CMA, and rotate the target such that the surface lies on

TABLE I. Representative ORNL ECR ion source beams (electrical μA); with the exception of the Ar and Kr beams, which were obtained for a 12-kV acceleration potential, all beam currents are quoted for a 10-kV source potential; unless otherwise indicated, 15×15 mm^2 charge analyzer slits were used, which corresponds to an analyzer acceptance of about 250π mm mrad. Asterisk indicates m/q degeneracy with contaminant beam.

	^{16}O	^{40}Ar	^{56}Fe	^{58}Ni	^{84}Kr	^{127}I	^{129}Xe[a]	^{181}Ta	^{197}Au
1+	400	110	10						
2+	300	120	*						
3+	170	90	20						
4+	100	75	*						
5+	83	*	23	3	20				
6+	50	65	25	5	25				
7+	2.5	73	*	7	26				
8+	0.1	105	*	12	27				
9+		45	20	20	33		5.0		
10+		*	10	17	31	8	4.5	12	25
11+		3.0	5	*	33	10	3.5	*	27
12+		0.7	*	5	40	14	3.5	12	21
13+			2	3	23	18	3.2	12	18
14+			*	1	21	20	2.5	12	*
15+			1.5	0.5	15	18	1.5	12	18
16+				0.15	5	*	1.2	12	15
17+				0.03	1	10	1.0	11	12
18+					*	*	0.6	8	10
19+					0.25	3	0.6	5	7
20+						2	0.5	3.5	5
21+						*	0.25	2	5
22+						0.5	0.12	1.8	4
23+								*	3
24+								1.5	2.5
25+							0.08	1.0	*
26+							0.05	*	0.9
27+								0.4	0.4
28+								0.1	*
29+								0.05	0.1
30+									0.015[b]
31+									0.005[b]

[a] 5×5 mm^2 slits.
[b] 2×2 mm^2 slits.

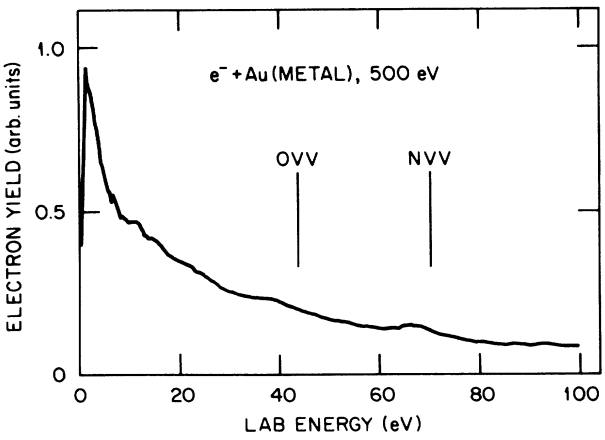

FIG. 1. Electron energy distribution corresponding to normal incidence 500-eV electron bombardment of a clean Au single crystal.

the CMA axis. Due to the cosine angular distribution of low-energy target emission,[10,11] such spectra contain predominantly electrons emitted from the projectile. Further, since only a small proportion of projectiles in our energy range are reflected from the target at normal angles of incidence, the electrons we see arise from the early part of the interaction of the multicharged ion with the surface.

III. EXPERIMENTAL RESULTS

The general characteristics of the electron energy distributions produced in the multicharged-ion–metal-target interaction are shown for Cu and Au targets and the projectiles N^{6+}, O^{7+}, and Ar^{9+} in Fig. 5. Each of these projectiles has the outer shell plus one electron removed. All spectra were obtained using the geometry of Fig. 2 (i.e., without slit), and are thus of low angular and

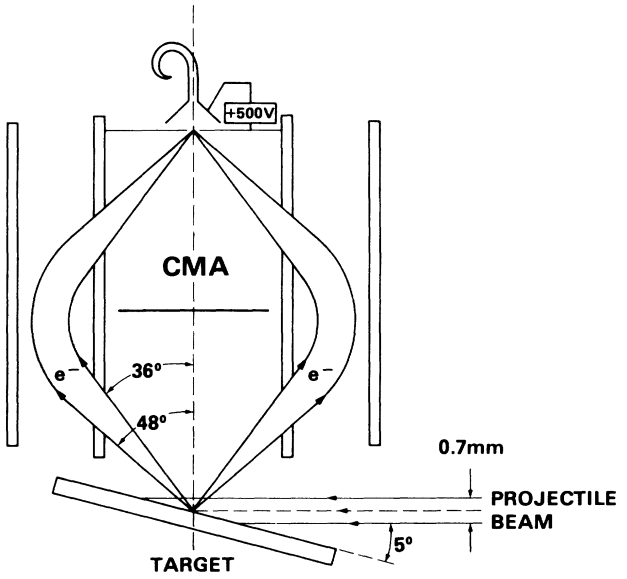

FIG. 2. Schematic illustration of the experimental and detection geometries used for the majority of measurements reported in this paper. The CMA axis is located at 90° to the incident ion beam direction. Acceptable detection efficiency for low-energy electrons is ensured by the use of Helmholtz coils to compensate the earth and laboratory magnetic fields, and an acceleration bias between the final aperture and detector.

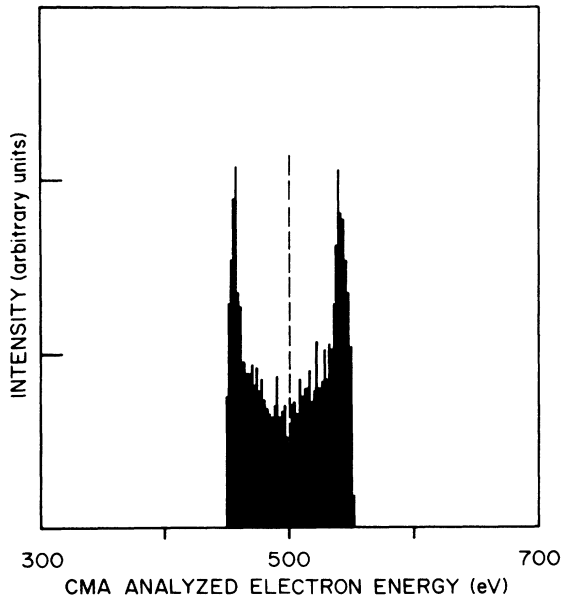

FIG. 4. Simulated Doppler profile corresponding to the CMA geometry of Fig. 2, and a moving 70-keV point source of oxygen *KLL* Auger electrons at the spectrometer focus. The electrons emitted are assumed to have, in the projectile frame, an energy of 500 eV and an isotropic angular distribution.

energy resolution. The intensity normalization is to measured crystal current (ion beam current plus electron emission). The spectra have not been corrected for CMA solid angle, absolute transmission, or absolute detection efficiency. The spectra *have* been corrected for the constant $\Delta E/E$ transmission of the CMA analyzer.

To first order, the electron emission spectra are composed of two peaks, a high-energy peak at the position expected for decay of the lowest-lying projectile vacancy, and a low-energy peak, with structure and intensity which is strongly dependent on target material. Most of the total intensity is contained in this low-energy peak.

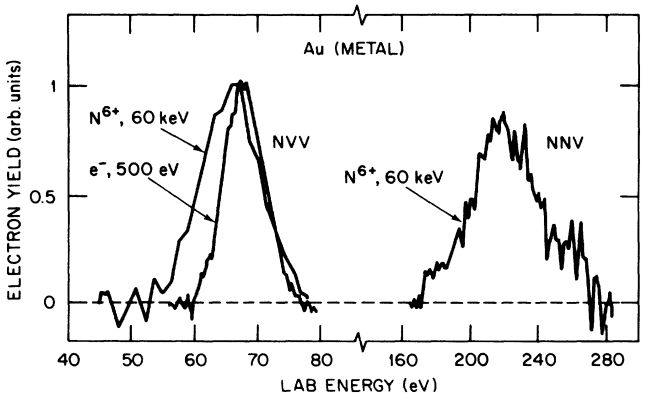

FIG. 3. Measured line profiles of the electron and multicharged-ion-induced *NVV* and *NNV* transitions of Au(metal). The widths and positions differ due to the different source sizes (see text). A monotonic background has been subtracted in each case.

If we correlate the high-energy peak with Auger electrons emitted by decay of the projectile core hole, these energetic electrons may scatter from the target electrons, leading to energy loss and secondary processes. The question arises, how much of the low-energy ion-induced peak can be attributed to such processes? To study this effect, we convolute the electron emission spectrum from Au under 500 eV electron impact (Fig. 6) with the instrumental resolution (assumed Gaussian with FWHM $=0.16E$) and Doppler profile appropriate to 500 eV electrons emitted from oxygen at 70 keV (Fig. 4). We assume two limiting cases in Fig. 7, namely, (1) projectile decay wholely outside the surface, and (2) decay inside the material. In the first case 50% of the ejected Auger electrons enter the forward hemisphere and strike the target; in the latter case all electrons interact with the target. The calculated spectra (Fig. 7) corresponding to these two cases must be interpreted with caution, since it is assumed in using the loss distribution of Fig. 6 that all electrons strike the surface at normal incidence. However, since then the electrons must be *backscattered* (and consequently suffer significant energy loss), the simulation must overestimate the contribution of this process to the total intensity at lower energies. We see from Fig. 7 that scattered projectile-Auger electrons therefore contribute at most a few percent to the low-energy peak. Note also that the instrumental and Doppler broadening are not

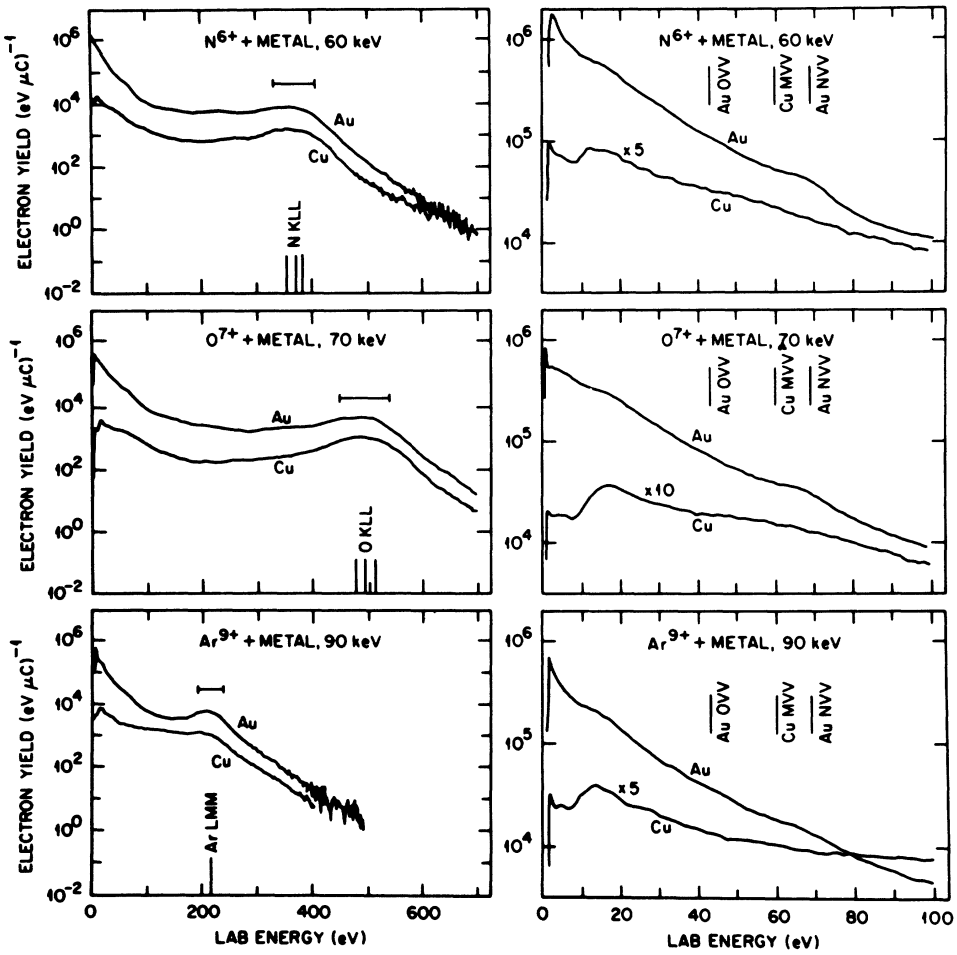

FIG. 5. Electron kinetic energy distributions corresponding to collisions of N^{6+}, O^{7+}, and Ar^{9+} projectiles with Cu and Au metal targets, for the geometry of Fig. 2. The instrumental resolution for features corresponding to a stationary emitter is $0.16E$. Emission from moving projectiles has an additional Doppler broadening $\Delta E = 2.7\sqrt{E_P E_T}$, where E_P is the electron energy corresponding to the projectile velocity, and E_T the emitted electron energy in the projectile frame. The resulting total widths are indicated by horizontal bars at the positions of the projectile *KLL* (O and N) and *LMM* (Ar) peaks.

sufficient to explain a significant electron yield at energies far exceeding the O *KLL* transition energy. Other processes must therefore be responsible for this emission.[14]

We see already in Fig. 5 the essential independence on projectile ion of the low-energy part of each spectrum for a given target. This similarity is demonstrated more clearly in Figs. 8 and 9, where the spectra for each target are normalized at the lowest-energy peak. The differences at higher energies can be attributed primarily to the varying overlap of the projectile core level decay contribution.

We expect one contribution to the intensity at low energy to arise from so-called secondary-electron emission. The emission spectra characterizing this process peak at about $\Phi/2$, where Φ is the metal work function.[11,12] At the very lowest energies (of order Φ), the form of the spectrum is expected to be independent of projectile and energy, and reflect a random electron cascade.[11] Toward higher energies, direct processes are expected to become more important, especially quasi-elastic-scattering of bound electrons in discrete states of the projectile or target from target or projectile atoms (promotion to the projectile or target continuum[15]). The energy spectrum for this process is well described by the empirical function

$$Y(E) \propto E^{-1} \exp(-\alpha E / v_p) , \tag{1}$$

where E is the emitted electron energy, v_p the projectile velocity, and α a constant depending on the collision partners.[15] This relation must be seen here as the "source function," which will be modified by transport through the solid target and surface potential barrier. Ideally, we should directly *measure* the form of this modified spectrum for bombardment of Cu and Au metals with neutral (or at most singly ionized) projectiles of the same kinetic energy as our multicharged species. Singly charged beams of energy greater than 20 keV are, however, not available from the ORNL ECR source. We

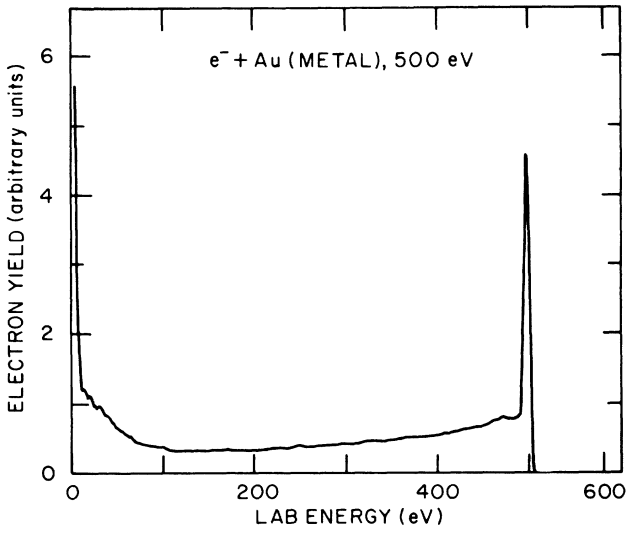

FIG. 6. Energy spectrum of 500-eV electrons scattered from Au(metal) for normal-incidence bombardment. Only a small fraction of the total intensity appears as elastically scattered electrons. The total intensity is dominated by secondary processes.

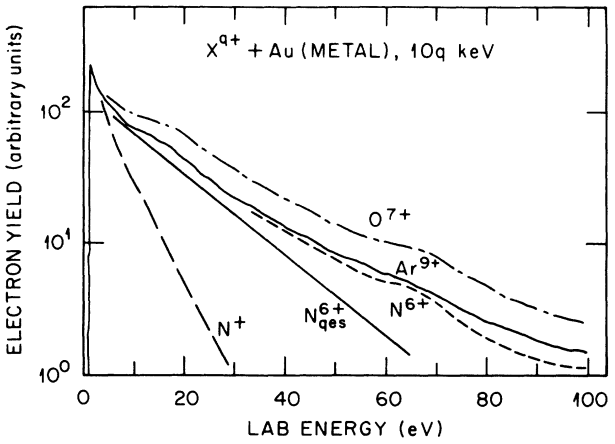

FIG. 8. Low-energy portion of the electron spectra emitted in the collision of O^{7+}, Ar^{9+}, N^{6+}, and N^{+} projectiles with Au(metal). The 10-keV N^{+} spectrum is used to determine the coefficient α in Eq. (1), which in turn was used to estimate the contribution of quasi-elastic-scattering processes ($N^{6+}{}_{qes}$) to the experimental N^{6+} spectrum. The experimental spectra are all normalized to the low-energy peak, and collected for the arrangement of Fig. 2.

are forced, therefore, to approximate the actual function by the "source function" and determine α in the above equation at an available beam energy, then use this scaling relation to estimate the contribution to our spectra of such processes. The result of such an analysis for N^{+} bombardment of Au is shown in Fig. 8. Clearly, the major portion of the electron emission in the energy region 0–100 eV can be attributed to secondary-electron cascades and quasi-elastic-scattering of bound electrons of the projectile or target. Apparently, the only major structures which remain to be explained are broad structures centered at about 20 and 70 eV for Au (Fig. 8), and 15 and 60 eV for Cu (Fig. 9).

Let us return to the possible mechanisms for electron emission in the multicharged-ion–metal interaction. The mechanism of Arifov *et al.* invokes transitions from the

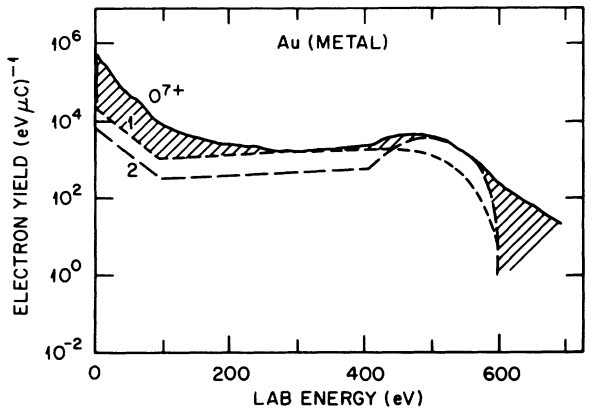

FIG. 7. Comparison of the measured ion-induced electron energy distribution for bombardment of Au(metal) with 70-keV O^{7+} and the arrangement of Fig. 2, and calculated spectra which could arise alone from projectile *KLL* electrons emitted either from decay of the *K*-shell vacancy outside the target, whereby only half of the Auger electrons strike the metal surface (curve 2) or by assuming the projectile has penetrated the surface before decay of the *K*-shell vacancy (curve 1). Further details of the simulation can be found in the text. The normalization of the spectra is arbitrary, and designed to demonstrate the maximum possible contribution of such *KLL* electron features to the observed ion-induced spectrum. The intensity in the shaded regions must therefore arise from other processes, not related to projectile *KLL* transitions.

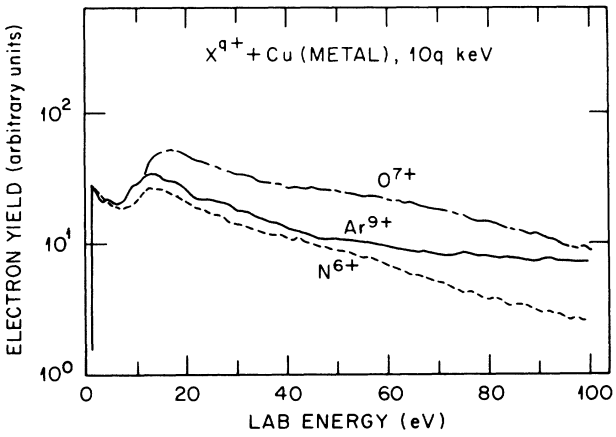

FIG. 9. Low-energy portion of the electron spectra emitted in the collision of O^{7+}, Ar^{9+}, and N^{6+} projectiles with Cu(metal). Normalization and experimental arrangement as in Fig. 8.

TABLE II. Auger electron peak positions in the energy range 0–300 eV in electron-induced emission spectra of Cu(metal) and Au(metal). The energy-level nomenclature is that used in Ref. 16.

Metal	Peak position[a] (eV)	Transition	Lower state lifetime (s) (Ref. 18)
Au	24	$N_{VII}/N_{VI}O_{III}O_{45+1}$	4×10^{-15}
	43	$O_{III}O_{45+1}O_{45+1}$	5×10^{-16}
	69	$N_{VII}/N_{VI}O_{45+1}O_{45+1}$	4×10^{-15}
	95	$O_{I}O_{45+1}O_{45+1}$	
	141	$N_{V}N_{VI}N_{VI}$	4×10^{-16}
	150	$N_{V}N_{VI/VII}N_{VII}$	4×10^{-16}
	160	$N_{IV}N_{VI}N_{VI}$	4×10^{-16}
	165	$N_{IV}N_{VI}N_{VII}$	4×10^{-16}
	184	$N_{V}N_{VII}O_{III}$	4×10^{-16}
	200	$N_{IV}N_{VI}O_{III}$	4×10^{-16}
	216	$N_{V}O_{I}O_{45+1}$	4×10^{-16}
	239	$N_{V}N_{VII}O_{45+1}$	4×10^{-16}
	255	$N_{IV}N_{VI}O_{45+1}$	4×10^{-16}
Cu	58	$M_3M_{45}M_{45}$	8×10^{-16}
	60	$M_2M_{45}M_{45}$	8×10^{-16}
	105	$M_1M_{45}M_{45}$	8×10^{-16}

[a]Position of minimum of differential spectrum feature (Ref. 17).

valence band of the metal either directly to projectile core levels, or via higher-lying discrete projectile states in resonance with the valence band. Since the Fermi energies of Cu and Au are similar, this model predicts, to first order, that the low-energy electron emission be characteristic of the projectile, but not the target type. This is contrary to our observations (Figs. 8 and 9). We therefore explore the possibility that the remaining low-energy emission arises principally from the decay of excited target vacancies.

Electron-induced Auger emission spectra of Cu and Au exhibit peaks at the energies shown in Table II. The ion-induced spectra from Au(metal) (Figs. 8 and 10) exhibit clear structures around 20, 70, and 220 eV, suggesting from Table II the creation of N_{VII}, N_{VI}, and N_V holes. The spectra from Cu(metal) (Fig. 9) for N^{6+} and O^{7+}, on the other hand, contain only a very broad structure near 60 eV, suggesting the possible creation of M_{II} and M_{III} vacancies, whose decay is perturbed by some factor not present in the electron excitation spectrum. These features do not arise principally from bombardment of target atoms by energetic projectile-Auger electrons. If this were the case, both the 43 and 69 eV Au peaks would be observed with comparable intensity (Fig. 1). We see no evidence for a discrete feature at 43 eV in any of our ion-induced electron distributions from Au. The origin of the peaks we do observe can be easily understood in terms of vacancy transfer to the target. A necessary condition for this is the existence of coupling of the relevant inner-shell levels via molecular-orbital pseudocrossings or quasiresonant Demkov processes at internuclear separations exceeding the distance of closest approach. We will discuss the origin of these peaks for the case of hydrogen-like projectiles (N^{6+},O^{7+}) interacting with Au. Applying the rules for construction of correlation diagrams,[19] it is found[7] that the strongly promoted $5f\sigma$ molecular orbital (MO) correlated to the projectile $1s$ level) and the weakly demoted $4p\sigma$ MO (correlated to the $N_{IV,V}$ levels in Au) exhibit a pseudocrossing (Fig. 11). Charge transfer at this crossing leads to creation of Au $N_{IV,V}$ vacancies which subsequently relax. The primary decay path is via Auger transitions of the type *NNV* leading to the emission of

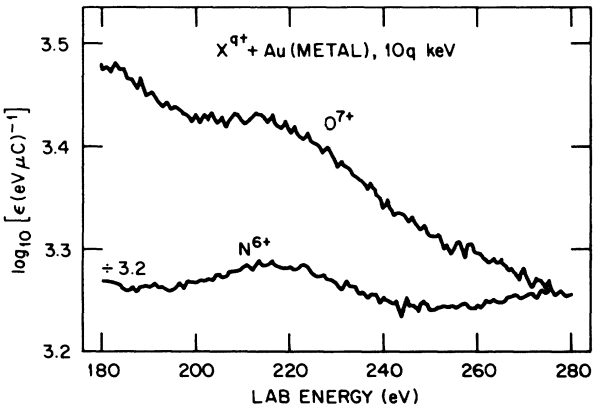

FIG. 10. Evidence for Au(metal) *NNV* transitions induced by bombardment of Au(metal) with O^{7+} and N^{6+} projectiles. The symbol ϵ refers to the electron yield.

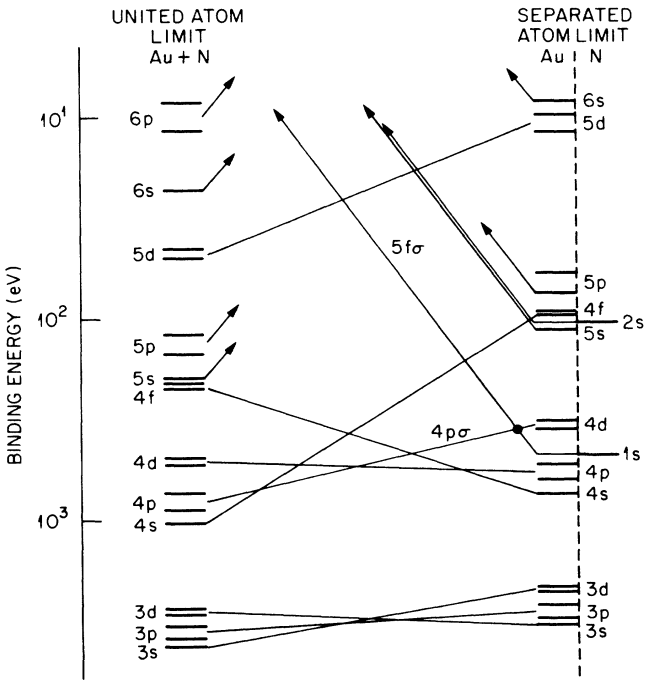

FIG. 11. Correlation diagram for the interaction of N^{6+} with Au, constructed using the diabatic correlation rules of Eichler *et al.* (Ref. 19). The correlation diagram for O^{7+} + Au is qualitatively similar, and also exhibits the pseudocrossing of the $5f\sigma$ and $4p\sigma$ MO's.

electrons with energies near 239 eV (Table II), and creation of $N_{VI,VII}$ vacancies. The latter subsequently decay, leading to the emission of the 24- and 69-eV features.

Further direct evidence that the peaks at 69 and 239 eV in the O^{7+} and N^{6+} spectra arise from transfer of K-shell vacancies which survive well into the interaction, and not from electron promotion in Au-Au collisions in the subsequent collision cascade, is provided by the electron energy spectra corresponding to projectiles in which the K shell is filled, namely, Li-like N and O. The 69- and 239-eV peaks are absent from such spectra. Further, Fig. 12 shows that the K-shell hole is not responsible for the remainder of the low-energy emission. This must arise then from the presence of the L-shell holes on the projectiles O and N, or other processes, such as that described by Eq. (1).

By considering the Coulomb interaction for this two-state vacancy transfer reaction and the asymptotic energy difference between initial and final states, the pseudocrossing is estimated to occur in the range 0.2–0.4 Å, which is well outside the distance of closest approach of 0.1 Å calculated for these collision systems. The lifetime of the initial Au $N_{IV,V}$ vacancy created in the collision is 4×10^{-16} s (Ref. 18) (Table II). The time scale t for the hard collision can be estimated using the relation $t\approx b(M/2E_p)^{1/2}$, where b is a measure of the size of the collision region, and M and E_p are the projectile mass and kinetic energy, respectively. For $b\approx0.4$ Å, $t\approx4\times10^{-17}s$ for 70 keV O^{7+}. Clearly then, this decay occurs after the projectile has left the collision region, and provided that secondary collisions of the target atom with other metal atoms involve on the whole significantly larger impact parameters, and sputtering is of minor significance, the decay spectra of perhaps the $N_{IV,V}$, and certainly the $N_{VI,VII}$ vacancies (lifetime 4×10^{-15} s, Table II), will be characteristic of an undisturbed Au atom in the solid state, and will therefore resemble electron-impact-induced spectra, as indeed we observe (Figs. 8 and 10).

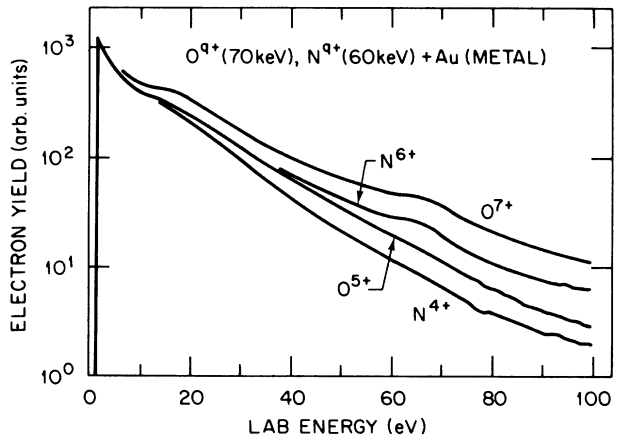

FIG. 12. Comparison of the electron energy spectra for bombardment of Au(metal) with hydrogenlike and lithiumlike projectiles, demonstrating the role of L-shell vacancies in the remaining low-energy electron emission.

Our observation of structures near 20, 70, and 220 eV from Au, and the absence of a peak at 43 eV, is consistent with this interpretation in terms of correlation diagrams.

It is noted that while projectile-Auger electron emission during multicharged-ion–surface collisions has been observed also by Delaunay *et al.*[20] and by de Zwart,[21] neither group was able to discern ion-induced target Auger electron emission. Both the measurements of Delaunay *et al.*, who studied N^{6+} and Ar^{9+} incident on W and Au, and those of de Zwart, who studied Ar^{9+} incident on W, were performed at significantly lower projectile energies. Delaunay *et al.* attribute the absence of ion-induced target Auger electrons in their spectra to almost complete filling of the projectile inner-shell vacancies at large internuclear separations before vacancy transfer can occur. Alternatively, it is possible that at the lower energies investigated the molecular pseudocrossings lie inside the distance of closest approach, and thus are no longer accessible in the collision. In the case of the W target, an additional possibility is that no favorable pseudocrossings exist to facilitate vacancy transfer. This may be the reason that de Zwart does not observe target Auger lines in his electron spectra acquired at 20 keV, at which energy most of the projectile L-shell vacancies are inferred to have survived the initial large-distance ion-surface interactions.

Let us now return to a consideration of Figs. 8 and 9. We have shown that the low-energy spectral features seem to be related to target emission. While we can explain the origin of several discrete features, and provide a qualitative estimate of the contribution of electron cascades and quasi-elastic-scattering processes to the remaining continuumlike background, we cannot exclude other emission processes. In particular, we have provided no explanation for the structure around 15 eV from Cu (Fig. 9). Before doing so, we wish to discuss the extreme width (up to 40 eV!) of such target features. Direct creation of target vacancies on the outer shells may easily result in shifted and broadened Auger "line" features. The perturbation may have two possible origins, namely, the possibility of multiple vacancy creation on a single target atom, and possible similar time scales for the collision and Auger decay. Thus both single or multiple vacancy transfer between higher-lying projectile and target discrete states via molecular-orbital pseudocrossings may in principle result in nondiscrete low-energy electron emission spectra. In this work the vacancy lifetimes are too long, so multiple vacancy transfer would appear to be responsible for, for example, the extreme width of the 60-eV structure which appears to exist in the spectra for O^{7+} and N^{6+} bombardment of Cu (Fig. 9).

To study the proposal that a portion of the almost structureless low-energy electron emission spectra correlates with the transfer of specific projectile inner-shell vacancies to target atoms, we performed a series of measurements, at constant projectile kinetic energy, for a range of charge states. We chose the series Ne^{7+}, Ne^{6+}, Ne^{5+}, which has vacancies in the energy region close to that of the upper 5s, 4f, and 5p levels of Au. Auger decay of these Au levels leads directly to electron emission in the energy region 0–100 eV. The results are shown in

Fig. 13, while in Fig. 14 the contribution to the electron emission of the Ne^{7+} and Ne^{6+} deepest-lying vacancies are derived by taking the difference of the curves for Ne^{7+} and Ne^{6+}, and Ne^{6+} and Ne^{5+}. These difference spectra exhibit features in this region which must be due to the presence of these specific projectile holes, in addition to the secondary and quasi-elastic-scattering emission (which is, of course, absent from the *difference* spectra). Some evidence for a component around 3 eV can also be seen, which corresponds to the energy region for capture to the projectile continuum. Due to the energy-dependent transmission function of the analyzer, however, this extreme low-energy region is very sensitive to an accurate determination of the background contribution to the spectrum for each projectile. The positions of the strongest transitions in the electron-induced Auger spectra from Au are shown in Fig. 14. One might thereby *tentatively* associate the observed structures with production of specific target vacancies on the 5*s*, 4*f*, and 5*p* shells. Such identifications, however, would be far from conclusive. Uncertainties in the rules for construction of correlation diagrams for the upper states of such an asymmetric collision system make a detailed analysis very difficult, and we do not attempt to do so. If the above interpretation is correct, however, such an analysis must show only a weak coupling of the lowest-lying Ne^{7+} projectile vacancy to the O_{III} level of Au, this level being responsible for 43-eV Auger electrons.

We can apparently provide a consistent explanation of all features of the electron emission from Au under multicharged-ion bombardment without invoking mention of the Arifov mechanism. This mechanism supposes that the projectile neutralization proceeds via a sequence of resonant and Auger captures of electrons from the metal valence band. If we compare the Fermi-surface parameters of Cu and Au (Table III), we observe that Cu has both a higher electron concentration and larger Fermi wave-vector magnitude. These factors lead for Cu to an enhanced tunneling probability between metal and

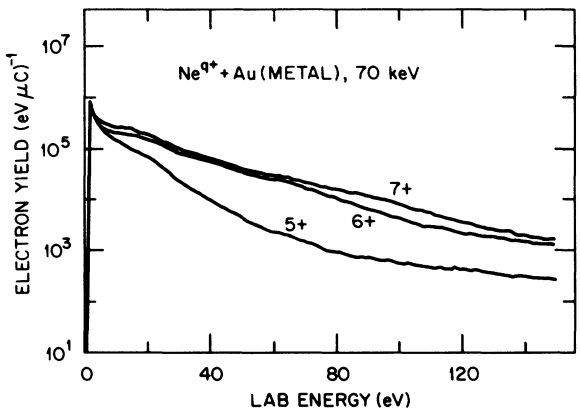

FIG. 13. Low-energy portion of the electron spectra emitted in the collision of Ne^{7+}, Ne^{6+}, and Ne^{5+} projectiles, at an energy of 70 keV, with Au(metal), for the experimental arrangement of Fig. 2.

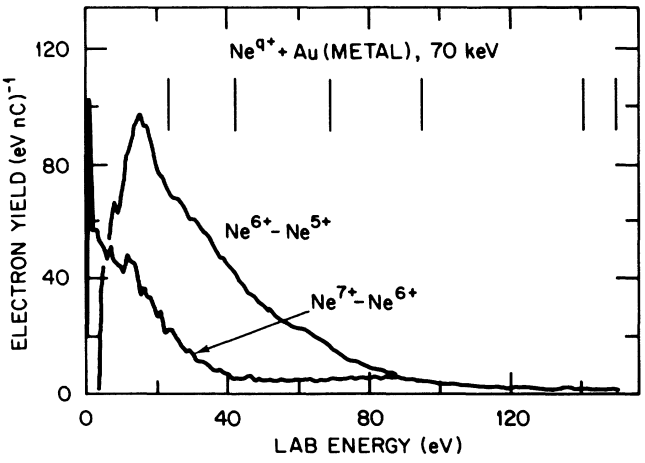

FIG. 14. Difference of the spectra of Fig. 13 for Ne^{7+} and Ne^{6+}, and Ne^{6+} and Ne^{5+}. These spectra show the contribution to the total electron spectrum of the respective vacancies on Ne^{7+} and Ne^{6+}. The positions of observed transitions in electron-induced Auger spectra of Au(metal) are indicated (from Table II).

projectile, and enhanced transition rate over that expected for Au. Thus we would expect to see more evidence for the Arifov mechanism in the spectra from Cu. Arifov *et al.*[5] predict Auger decay steps of order 15–30 eV. This leads, for filling of the projectile outer shells, to observed Auger electron energies of order 15–30 eV minus twice the metal work function. The data from both Cu and Au indeed exhibit a structure in this energy region (5–20 eV). While that from Au may be explained as above (at least in part) by decay of an N_{VII} or N_{VI} vacancy on Au atoms, we can provide no similar explanation for such a peak from Cu (see Table II). We propose that

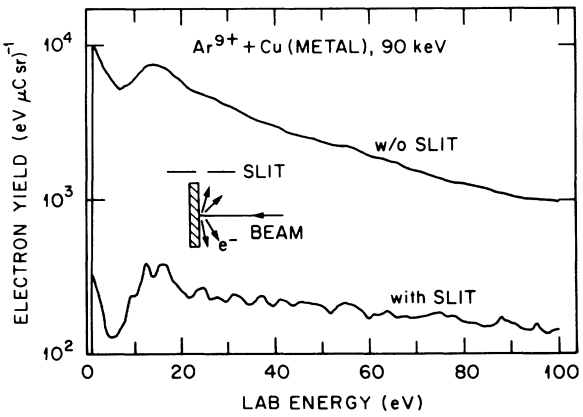

FIG. 15. Comparison of the low-energy electron spectra emitted in the collision of Ar^{9+} with Cu(metal) at normal incidence. The angular aperture for the spectrum "with slit" covers the range 0°–8° to the surface plane, and "without slit" the range 0°–48°. The experimental geometry is shown in the inset. The spectra have been normalized to the same effective analyzer solid angle.

TABLE III. Calculated free-electron Fermi-surface parameters for metals (Ref. 22).

Metal	Valency	Electron concentration (cm^{-3})	Fermi energy (eV)	Fermi wave vector (cm^{-1})
Cu	1	8.45×10^{22}	7.0	1.36×10^{8}
Au	1	5.90×10^{22}	5.51	1.2×10^{8}

at least this peak arises from Auger decay of projectile vacancies via the Arifov mechanism.

To study this hypothesis in more detail, we examine in Fig. 15 the angular dependence of the low-energy electron emission from Cu under Ar^{9+} bombardment. We have normalized the spectra in Fig. 15 to the same effective detector solid angle. Features of the emission spectrum characteristic of electrons emitted from the target will be strongly depressed at ejection angles near parallel to the surface, due to the cosine angular dependence of such emission.[10,11] The peak at 15 eV indeed does not reduce in the same proportion as the secondary-electron emission peak at 2 eV. This suggests that electrons in the 15-eV peak have not been ejected over a planar potential barrier. We propose these electrons arise from one-center Auger decay of excited projectile ions above the surface. The angular dependence thus provides evidence that capture of metal valence electrons to projectile excited states does occur in some instances, followed by Auger decay of these states, before the projectile penetrates the surface layer.

It is noted that the spectra of Fig. 15 were taken with the ion beam at normal incidence, and consequently at significantly higher perpendicular velocities than the grazing incidence spectra discussed earlier. Due to this difference in experimental conditions, the conclusion reached on the basis of Fig. 15 may not apply to grazing incidence bombardment.

IV. CONCLUSION

We have measured electron kinetic energy distributions arising from the interaction of $\approx 10q$-keV multicharged ions with metal surfaces. At these energies, the major contribution to the total yield arises from emission from the target. The spectra at low energies contain a contribution which we identify with secondary-electron emission and quasi-elastic-scattering processes (electron promotion to the target or projectile continuum). Superimposed on this is emission correlating with decay of projectile vacancies, and emission correlating with decay of both unperturbed and strongly perturbed target vacancies. The creation of target vacancies implies that a measurable fraction of projectile vacancies survives until small-impact-parameter collisions with a surface or subsurface target atom. Our data imply that the neutralization proceeds via two channels, viz., capture of valence-band electrons to projectile excited states, followed by one-center Auger decay, and at pseudocrossings of molecular orbitals correlating with discrete inner-shell levels of the target and projectile. We have insufficient information to permit an estimate of the relative importance of these two neutralization paths. The initial vacancies, if transferred to target atoms, decay, leading to electron spectra characteristic of the target. Depending on the vacancy lifetime, such vacancies decay either unperturbed, or in the field of the projectile, leading to discrete or broadband emission, respectively. Line shifts will also arise if multiple vacancy transfer to a single target atom occurs. Deep-lying projectile vacancies may also be transferred via this mechanism. Conclusive evidence for this was presented for K-shell vacancies of N and O. We recommend that future experiments be performed using lower-Z target materials, which are more amenable to quantitative theoretical analysis.

ACKNOWLEDGMENTS

It is a pleasure to acknowledge valuable discussions with J. Burgdörfer, R. Janev, R. A. Phaneuf, and N. Stolterfoht. One of us (K.J.S.) wishes to thank the Physics Division, ORNL, for hospitality and support, Dr. J. Noonan for assistance with preparation of the Cu crystal, and G. Ownby and J. Hale for skilled technical assistance. This work was supported by the Division of Chemical Sciences, U.S. Department of Energy, under Contract No. DE-AC05-840R21400 with Martin Marietta Energy Systems, Inc. Support for K.J.S. was also provided by the Deutsche Forschungsgemeinschaft.

*Permanent address: Fachbereich Physik, Universität Osnabrück, 4500 Osnabrück, West Germany.

[1]U. A. Arifov, E. S. Mukhamadiev, E. S. Parilis, and A. S. Pasyuk, Zh. Tekh. Fiz. **43**, 375 (1973) [Sov. Phys.—Tech. Phys. **18**, 240 (1973)].

[2]P. Varga, W. Hofer, and H. Winter, Surf. Sci. **117**, 142 (1982).

[3]S. T. de Zwart, T. Fried, U. Jellen, A. L. Boers, and A. G. Drentje, J. Phys. B **18**, L623 (1985).

[4]M. Delaunay, M. Fehringer, R. Geller, D. Hitz, P. Varga, and H. Winter, Phys. Rev. B **35**, 4232 (1987).

[5]U. A. Arifov, L. M. Kishnevskii, E. S. Mukhamadiev, and E. S. Parilis, Zh. Tekh. Fiz. **43**, 181 (1973) [Sov. Phys.—Tech. Phys. **18**, 118 (1973).

[6]P. Varga, W. Hofer, and H. Winter, Scanning Electron Microsc. **1**, 967 (1982).

[7]F. W. Meyer, C. C. Havener, K. J. Snowdon, S. H. Overbury,

D. M. Zehner, and W. Heiland, Phys. Rev. A **35**, 3176 (1987).
[8]R. L. Erickson and D. P. Smith, Phys. Rev. Lett. **34**, 297 (1975).
[9]F. W. Meyer, Nucl. Instrum. Methods B **9**, 532 (1985).
[10]R. Bindi, H. Lanteri, P. Rostaing, and P. Keller, J. Phys. D **13**, 2351 (1980).
[11]J. Schou, Phys Rev. B **22**, 2141 (1980).
[12]W. Steckelmacher, J. Phys. E **6**, 1061 (1973).
[13]V. V. Zashkvara, M. I. Korsunskii, V. P. Lavrov, and V. S. Red'kin, Zh. Tekh. Fiz. **41**, 187 (1971) [Sov. Phys.—Tech. Phys. **16**, 141 (1971)].
[14]K. J. Snowdon, C. C. Havener, F. W. Meyer, S. H. Overbury, and D. M. Zehner (unpublished).
[15]P. H. Woerlee, Yu. S. Gordeev, H. de Waard, and F. W. Saris, J. Phys. B **14**, 527 (1981).
[16]W. A. Coghlan and R. E. Clausing, Oak Ridge National Laboratory Report No. ORNL-TM-3576, 1971.
[17]*Handbook of Auger Electron Spectroscopy,* edited by Lawrence E. Davis, Noel C. MacDonald, Paul W. Palmberg, Gerald E. Riach, and Roland E. Webber (Perkin-Elmer Corporation, Eden Prairie, 1980).
[18]J. C. Fuggle and S. F. Alvarado, Phys. Rev. A **22**, 1615 (1980).
[19]J. Eichler, U. Wille, B. Fastrup, and K. Taulbjerg, Phys. Rev. A **14**, 707 (1976).
[20]M. Delaunay, M. Fehringer, R. Geller, P. Varga, and H. Winter, Europhys. Lett. **4**, 377 (1987); P. Varga, M. Delaunay, M. Fehringer, R. Geller,and H. Winter, *Abstracts of Contributed Papers, Fifteenth International Conference on the Physics of Electronic and Atomic Collisions, Brighton, United Kingdom, 1987,* edited by J. Geddes, H. B. Gilbody, A. E. Kingston, and C. J. Latimer (North-Holland, Amsterdam, 1988), p. 793.
[21]S. T. de Zwart, Nucl. Instrum. Methods B **23**, 239 (1987); Ph.D. thesis, University of Groningen, 1987.
[22]C. Kittel, *Introduction to Solid State Physics,* 4th ed. (Wiley, New York, 1971), p. 248.